ELSEVIER

Chemical Engineering Journal 80 (2000) 141–148

Chemical Engineering Journal

www.elsevier.com/locate/cej

Consolidation and aggregate densification during gravity thickening

J.B. Farrow*, R.R.M. Johnston, K. Simic, J.D. Swift

AJ Parker CRC for Hydrometallurgy, CSIRO Minerals, PO Box 90, Bentley, WA 6982, Australia

Abstract

A continuous laboratory column system has been used to investigate the consolidation behaviour of kaolin slurries flocculated by a nonionic flocculant under different conditions. Measurements of the steady-state bed density profile showed that higher agitation intensities during flocculation resulted in lower bed densities. The relative importance of compression versus shear for kaolin dewatering was determined by operating the steady-state column system at different bed heights above a mechanical rake. It was found that rake action, not compression, was the dominant dewatering mechanism. Samples taken from the consolidating bed before and after the rake were analysed by microscopy to determine the density–size relationship of the individual aggregates. This showed that the dewatering induced by the rake action occurred not only by removal of inter-aggregate liquor but also by densification of the aggregates (i.e. removal of intra-aggregate liquor). Measurements made on full-scale thickeners are also presented which demonstrate similar behaviour.

Keywords: Flocculation; Continuous column; Compression; Raking

1. Introduction

Gravity thickening is widely used in the mineral processing industry as the prime technology for solid–liquid separation. The requirement from gravity thickening varies, with thickeners being used: (i) to produce clarified liquor for further processing (e.g. crystallisation); (ii) for counter-current leaching or washing; or (iii) to produce dense sediments for disposal.

A number of researchers have studied gravity thickening in continuous laboratory or pilot-scale columns, with diameters ranging from 9.5 to 97 cm and heights from 100 to 350 cm. Galvin and Waters [1] used both batch and continuous raked columns to determine settling flux curves for flocculated coal slurries. Comings [2] compared steady-state thickening operation of a model column with batch tests commonly used to specify settling area (i.e. thickener design capacity). Others researchers [3–6] used flocculated and unflocculated feed to examine the response to transient flows. Suspended picket fence rotors have been employed by some to prevent wall effects, with and without a bottom rake. Kos [7] used flocculated water treatment sludge in a 2.5 m column and set criteria for recognition of steady-state. He reported that days were required to reach steady-state and measured concentration and pressure profiles with respect to depth in the column. The objectives of these studies ranged from establishing limiting flux values and modes of column overload to numerical model validation. However, in all studies little if any attention was paid to the very important issue of the initial flocculation state and the use of reproducible flocculation conditions.

The important linkages between flocculation conditions, aggregate structure, sedimentation and subsequent dewatering performance of mineral suspensions are becoming more apparent [8,9]. For a given system (substrate, liquor, flocculant type and dosage) significant differences arise in the flocculation state (i.e. aggregate properties) when flocculation is conducted under different physical conditions. Factors such as solids concentration and the intensity and duration of agitation during flocculation have a profound influence on the resultant flocculation state [10].

This paper outlines dewatering results obtained from a continuous laboratory column where the feed suspension was flocculated under selected, reproducible agitation conditions. This has enabled the influence of agitation during flocculation on consolidation behaviour to be investigated. It has also allowed prolonged operation under steady-state conditions, so that the effect of bed height on the bed density profile could be established.

The raked column system used in this work closely approximates the forces (gravity, drag, network resistance) which consolidating sediments experience in industrial mineral processing thickeners. However, unavoidably there are significant experimental differences associated with the relative scale (e.g. wall effects, overburden weights, etc). For this

* Corresponding author. Tel.: +61-8-93348020; fax: +61-8-93348001.
E-mail address: john.farrow@minerals.csiro.au (J.B. Farrow).

1383-5866/00/$ – see front matter
PII: S1383-5866(00)00083-6

reason, results obtained from the laboratory column system have been compared with measurements made on full-scale thickeners to verify important observations.

2. Experimental

2.1. Kaolin feed suspension preparation

Kaolin (RF grade, Commercial Minerals, Australia) was used as the feed suspension for all laboratory column studies. The specific gravity was 2.68 g cm^{-3}, with a moisture content of 3.9 wt.% (from drying at 70°C).

Preparation of the kaolin feed slurry involved soaking 13.2 kg of kaolin in deionised water (slurry concentration: ≈16 wt.%) for 24 h, followed by 24 h of recirculation (≈130 l min^{-1}) through an in-line static mixer (Sulzer SMV4 DM25) using an impeller pump. The treated slurry was then transferred to the column feed tank and diluted with deionised water on a weight/volume basis to produce 300 l of feed containing 44 g l^{-1} kaolin.

Without this pre-treatment, the kaolin's particle size slowly decreased over the 24 h holding time. This significantly affected the flocculation characteristics of the feed suspension, resulting in a drop in the settling rate achieved at a flocculant dosage of 250 g t^{-1} from 11 to 6 m h^{-1} over the 24 h holding time. Use of the slurry preparation procedure described resulted in a stable particle size within the holding tank (Table 1) and hence enabled constant flocculation conditions and steady-state conditions for the column.

2.2. Flocculant preparation

A nonionic ultra-high molecular weight polyacrylamide flocculant (M333, Allied Colloids) was used for the laboratory column studies. Flocculant solutions (0.005 wt.% active) were prepared daily by dilution of a 0.5 wt.% flocculant solution with deionised water. A consistent mixing procedure was used for the preparation of the diluted flocculant. The 0.5 wt.% solution was prepared with deionised water (according to the manufacturer's specifications) every 20 days allowing at least 3 days for full solvation prior to use. It was stored in the dark at 4°C.

2.3. Continuous laboratory column system

A schematic of the continuous laboratory column system is shown in Fig. 1. The central perspex column is 123 mm in diameter and 1700 mm high. This column diameter was considered to be sufficient to minimise wall effects, although a larger diameter would always be preferable. However, with a larger diameter the quantities of feed slurry required to operate the system on a continuous basis become excessive for laboratory operation.

The column was operated continuously over periods of several weeks. Batches of kaolin feed suspension were prepared daily as described above, and added to the main feed holding tank. Feed slurry was pumped from the main holding tank into a secondary feed tank, which served as a buffer during periods of refilling the main feed tank.

The use of the Shear Vessel for inducing flocculation under reproducible conditions has been described previously [11]. The Shear Vessel consists of an inner rotating cylinder (200 mm diameter) within a stationary outer cylinder (210 mm diameter). Feed slurry was introduced at the top of the vessel. Flocculant entered through the side wall at a selected position depending upon the desired time for the flocculated suspension to experience the agitation induced by rotation of the inner cylinder. The rotation rate of the inner cylinder controls the agitation intensity experienced during flocculation. In all experiments reported here, the flocculant was introduced through the side wall 85 mm above the commencement of the tapered base.

Flocculated suspension exited from the Shear Vessel into the sedimentation column to settle onto the surface of the bed. A simple two-prong variable speed rake (60 mm high, operated at 2 rpm) at the base of the sedimentation column assisted with underflow discharge, via an opening in the side wall.

The entire system was controlled using the LabVIEW software package (National Instruments, USA) run on a Macintosh SE computer, monitoring the four peristaltic pumps and recording the height of the bed (determined from the output of five movable proximity sensors spaced 5 mm apart).

Sampling valves were located down the sedimentation column, 20 cm apart. Approximately 25 cm^3 was removed when determining solids concentration. Underflow samples were obtained from a sampling point located in the underflow line prior to the pump.

Extensive tests were conducted to confirm that representative feed solids were withdrawn from the main feed tank and the secondary feed tank at different slurry levels. The flow rates achieved using the peristaltic pumps were checked regularly. Achievement of steady-state conditions was assessed from a comparison (on a mass basis) of the solids removal

Table 1
Changes in kaolin particle size during feed slurry preparation

Sampled	d_{10} (μm)	d_{50} (μm)	d_{90} (μm)
Kaolin in water (24 h)	1.5	6.0	36.4
After 24 h recirculation through in-line static mixer	1.0	3.6	33.0
After 24 h recirculation through in-line static mixer, then 24 h stirring in the main feed tank	1.1	3.7	31.7

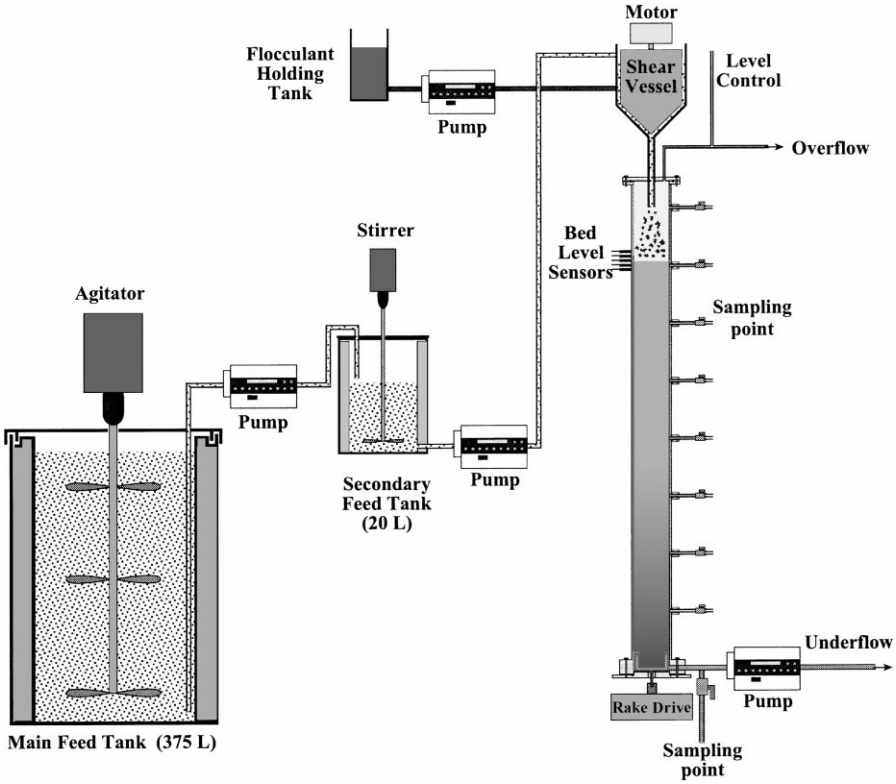

Fig. 1. Schematic of continuous laboratory column system.

rate versus the feed rate, and from the stability of the bed height. The system was run at steady-state conditions for at least one turnover time of the bed before samples were taken of the underflow and from within the bed. The solids concentration (as wt.%) of the samples was determined by drying at 70°C to constant weight.

2.4. Determining aggregate density

The density of individual aggregates present within different sediments was determined using a simple optical technique [12]. A schematic of the equipment, termed a floc density analyser (FDA), is shown in Fig. 2.

Sediment sample was diluted with corresponding filtered supernatant to a solids content of ≈ 0.2 wt.%. This required the application of agitation to the sediment, but this was as quiescent as possible to minimise unavoidable aggregate rupture. The dilute suspension was thermostatted at 25°C, then added to the analysis cell of the FDA (Fig. 2) and the taps closed to completely isolate the suspension to produce convection free settling. The settling characteristics of individual aggregates were recorded using a video camera fitted

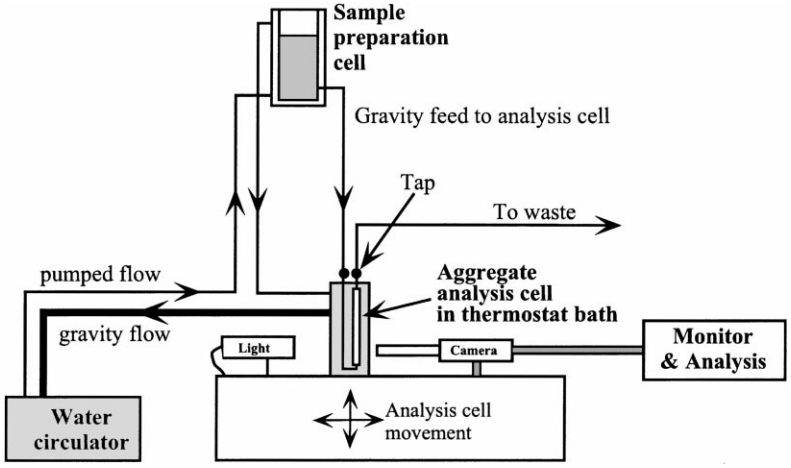

Fig. 2. Schematic diagram of the floc density analyser used to determine the size, settling rate and density of individual aggregates.

with a high magnification optical system (apparent magnification range 5 to ≈600 times).

The size of individual aggregates was determined by assuming an overall ellipsoidal shape defined by the maximum horizontal and vertical dimensions (with respect to the direction of settling). The diameter (D) of the sphere which had a Stokes settling velocity equivalent to the ellipsoid was determined using the expressions given by Happel and Brenner [13].

The aggregate settling velocities were assumed to be described by Stokes Law, which allows the calculation of the effective density from knowledge of the size, settling velocity and the viscosity and density of the fluid.

The relationship between the effective density and the size of aggregates is often [14–16] described by:

$$\rho_a = AD^{-n} + \rho_1 \quad (1)$$

where A and n are constants depending upon the aggregation state of the system.

It follows that the relationship between aggregate settling rate and aggregate size can be described by an expression of the form:

$$U_a = KD^x \quad (2)$$

where K and x are constants depending upon the aggregation state of the system.

Results from FDA measurements are presented as fitted curves, of the form of Eq. (1) or Eq. (2), since the high degree of scatter inherent in FDA data makes comparisons between sets of raw data very difficult. The scatter is due to the polydisperse nature of the primary particles (both size and density) present in mineral samples, plus the extreme asymmetric shape of aggregates formed by flocculation (see examples in Farrow and Warren [12]).

2.5. Determining bed density profiles within full-scale thickeners

The principle of operation of the natural γ-ray gauge used to determine the steady-state bed density profiles within full-scale thickeners has been described in detail elsewhere [17–19]. It measures the solids concentration of the sediment from the level of natural radioactivity contained in the constituent minerals, using a string of Geiger–Mueller counters. The intensity of this radiation is well below that of the cosmic background that would be registered in air. However, the large mass of the water in the thickener is an effective cosmic shield which enables the natural activity of the mud to be detected. The counters are located at set levels within a supporting steel sheath, inserted vertically into a thickener.

In this work, calibration of the gauge was conducted using a series of known concentrations of slurry (red mud) taken from the washer stage of the Bayer process. The measurements of counts versus solids concentration obtained in a well-mixed tank had a linear relationship.

In the Bayer process thickener, the counting time of the natural γ gauge was short in comparison with the period of rake rotation. Thus the gauge could be raised and lowered by a motorised winch to clear each passage of the rake arm, while maintaining the desired counting accuracy.

3. Results and discussion

3.1. Laboratory column experiments

3.1.1. Selection of operating conditions

The operating conditions of the laboratory column system were selected to roughly approximate those within a full-scale mineral processing thickener, 72 m in diameter with a throughput of 5000 m^3 per h (i.e. ≈1.23 $m^3\ m^{-2}\ h^{-1}$) at an average feed solids concentration of 50 g l^{-1}. Thus, the required feed flow to the laboratory column (cross sectional area 0.0119 m^2) to approximate the full-scale thickener would be 243 ml min^{-1}. However, a feed rate of 200 ml min^{-1} at a solids concentration of 44 g l^{-1} was used for convenience of refilling the main holding tank every 24 h.

3.1.2. The effect of agitation intensity during flocculation on consolidation behaviour

The effect of agitation intensity during flocculation on sediment compressibility during steady-state thickening in the laboratory column was examined using a flocculant dosage of 45 g t^{-1} at different Shear Vessel rotation rates (80–175 rpm). The steady-state bed profiles obtained under these conditions are shown in Fig. 3.

Different underflow rates, ranging from 41 to 51 ml min^{-1}, were required to maintain the constant bed height (1.5 m) under the different flocculation conditions due to the variations in the underflow density. It can be seen that the bed density at a given depth decreases with increasing agitation intensity used during the flocculation of the kaolin. The change in shape from one profile to the next

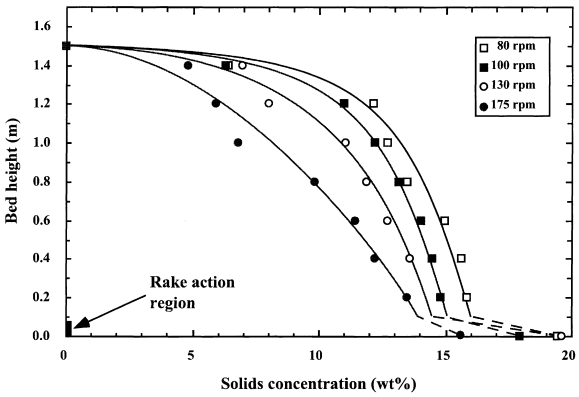

Fig. 3. Solids concentration as a function of bed depth obtained when different agitation intensities (i.e. Shear Vessel rotation speeds) were used during the initial flocculation of the suspension. Feed solids concentration 44 g l^{-1}, flocculant dosage 45 g t^{-1}.

must reflect the impact of differences in the structure of the aggregates formed at the different agitation intensities.

The mass of overburden (proportional to the area under the profile at any given bed height) required to compress each bed to a given solids concentration increased with agitation intensity used during flocculation. However, the drag within the beds also increased in the same order, since higher underflow rates were required with higher agitation intensities due to the corresponding fall in underflow density. From these data alone, the two effects cannot be separated to decide what fraction of the submerged weight of the overburden is counteracted by the drag and what fraction remains to compress the sediment network.

All density profiles, especially those obtained at lower agitation conditions, approach a limiting solids concentration with increasing bed depth. For example, the profile obtained when flocculation was conducted at a Shear Vessel speed of 80 rpm approaches a limiting solids concentration of ≈ 16 wt.%. However, the measured underflow density (plotted at 0 m bed height) was much higher (19.5 wt.%) which cannot be explained by the additional bed depth compared to the last sampling point. It is clear that the mechanical action of the rake at the base of the column has induced significant densification of the sediment. This demonstrates that both mechanical (shear) forces and compressive forces have important roles in the formation of high underflow densities from continuous columns.

3.1.3. The effect of bed height on consolidation behaviour

Different bed heights were established, at steady-state, in the continuous column by setting different underflow rates. The kaolin feed was flocculated using a flocculant dosage of 122 g t^{-1} and a Shear Vessel rotation speed of 150 rpm.

The solids concentration profiles (Fig. 4) were similar for the different height beds, with compaction at the bottom being the greatest with the highest bed. A significant increase in solids concentration at the base of the bed in the region of the rake was observed, consistent with the results presented in Fig. 3. These data are remarkably similar to the profiles

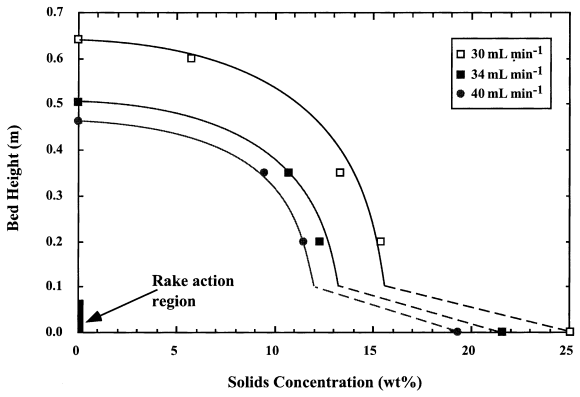

Fig. 4. The solids concentration profiles for different height beds achieved in the continuous column system using different underflow pump speeds.

(including the rake effect) obtained by Comings [2] in his study of the consolidation behaviour of unflocculated (but probably coagulated) calcium carbonate suspensions using a continuous 193 mm ID column and beds ranging from 0.22–1.20 m in height.

Since the same flocculation conditions were used in each case (Fig. 4), the product aggregates would all have had similar structures, i.e. size-density relationship and bond strength. Thus the compressive yield strength of the sediment network in each case would be expected to be similar. The hydrodynamic drag, however, which together with the network pressure supports the submerged weight in resisting compaction, depends on the underflow rate and would be highest for the lowest bed. This can be seen from the fact that a solids concentration of 10 wt.%, for example, was reached at a different depth in each case, requiring a greater overburden as the bed height decreased (≈ 0.11 m for the 0.65 m bed, ≈ 0.12 m for the 0.50 m bed and ≈ 0.15 m for the 0.46 m bed).

3.1.4. Mechanism of rake induced sediment densification

The role played by thickener rakes is generally considered only in terms of moving the consolidated sediment to a discharge point. However, as the data in Figs. 3 and 4 show, rakes can also play an important role in the compaction of flocculated suspensions through the mechanical force which is applied to induce sediment movement.

Confirmation that it was indeed the rake causing these effects was obtained from a similar experiment to those outlined above. The kaolin feed was flocculated at a dosage of 122 g t^{-1} at a Shear Vessel speed of 150 rpm, and the underflow pump rate set to establish a 1.2 m bed. After steady-state conditions were established, the rake was turned off. The bed rose to ≈ 1.6 m because of a fall in underflow density, from 19.5 wt.% to ≈ 12 wt.% (although the latter value was quite variable). Once the bed stabilised at its new position, the rake was turned back on and the bed fell, due to the increase in underflow density induced by the rake action.

Evidence for the mechanism of the bed compaction by rake action was obtained from FDA measurements made on individual aggregates present in the sediment, before and after the rake region.

Samples were taken from four points down the column during steady-state operation when the bed height was stable at 0.5 m (this was a similar, but separate, experiment to that shown in Fig. 4). The four sampling points were:

Position 1: from the Shear Vessel discharge (i.e. before entering the bed).

Position 2: at a bed depth of 0.3 m (bed solids concentration 13.6 wt.%).

Position 3: before the underflow pump (bed solids concentration 21.0 wt.%)

Position 4: after the underflow pump (solids concentration 21.0 wt.%).

The settling characteristics of approximately 200 aggregates in each sample were analysed. Fig. 5 shows the derived

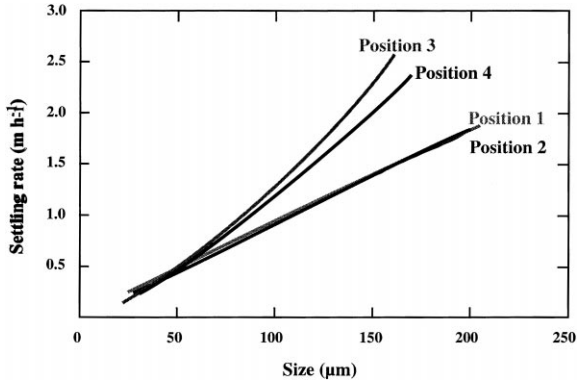

Fig. 5. Settling rate versus size of particles for samples taken from the column system at different positions.

aggregate settling rate versus aggregate size curves based on Eq. (2). Aggregates larger than ≈ 60 μm in the samples from position 3 and 4 had, on average, significantly faster settling rates than equivalent sized aggregates in the samples from positions 1 and 2. This implies that the samples from positions 3 and 4 contained aggregates having denser structures than those present in samples taken from positions 1 and 2, as illustrated by the derived aggregate density information given in Fig. 6.

It is notable that aggregates from positions 1 and 2 were almost identical, showing that the passage through the bed down to a depth of 300 mm had not substantially altered their structure from that formed during flocculation. This is evidence that the initial compaction of the bed, down to 13.6 wt.% solids, is due almost entirely to closer packing of individual aggregates and a loss of inter-aggregate liquor. Such a result is consistent with the reduction in the hydrodynamic (drag) component of network support which occurs as the bed approaches the bottom of the column and the solids settling velocity relative to the liquid decreases. At the bottom of the bed and in the underflow line, the relative velocity between the sediment and the liquid becomes zero and the drag disappears. Below ≈ 300 mm, with profiles as steep as those shown in Figs. 3 and 4, it is clear that the rake has been responsible for most of the additional dewatering.

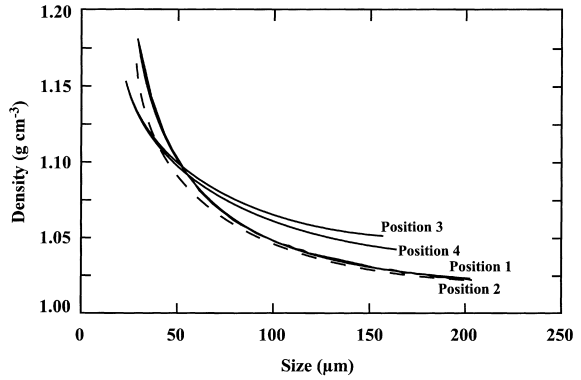

Fig. 6. Density versus size of particles for samples taken from the column system at different positions.

The aggregate density information (Fig. 6) can be used to calculated the apparent porosity of the aggregates. To explain their respective effective densities, the 150 μm aggregates from positions 1 and 2 would need to comprise 50 parts water to one part solid, whereas 150 μm aggregates from positions 3 and 4 would need to comprise ≈ 30 parts water to one part solid. In other words, the action of the rake removes about 40% of the intra-aggregate liquor under these laboratory conditions.

These results demonstrate that mechanical forces, such as those due to rake action, can be extremely important in aggregate densification. The mechanism can be attributed to a massaging action induced by the mechanical shear which disrupts or rearranges flocculant bonds between primary particles to form more compact aggregate structures or fragments which result in the release of some intra-aggregate liquor. The data in Figs. 5 and 6 suggest that the underflow pump has caused a slight reversal of dewatering, but this is considered due to experimental error in the data.

The rake used in the column experiments was not specifically designed to provide any particular form of mechanical action. Despite this, 40% of the intra-aggregate liquor in 150 μm aggregates was removed by the rake in the bottom 65 mm of the column. Improved rake design would presumably result in an even greater reduction of this internal liquor. Removal of intra-aggregate liquor, trapped within the aggregate structure during flocculation, is essential for forming high density underflows which have acceptable rheological properties.

3.2. Full-scale thickener measurements

3.2.1. Bed density profiles

The steady-state bed density profile measured using the natural γ-ray gauge within a full-scale thickener is shown in Fig. 7. The right hand figure is a schematic showing

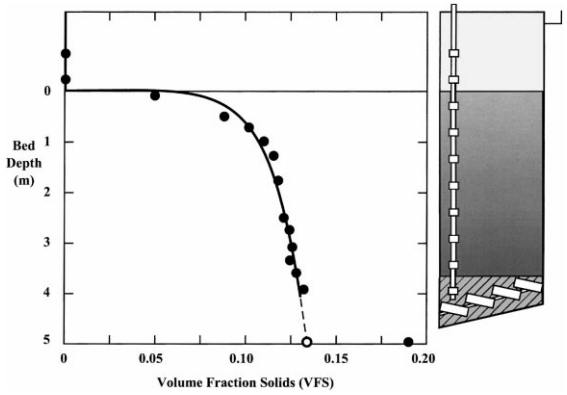

Fig. 7. Steady-state bed density profile within a full-scale continuous tailings thickener obtained using the gamma-ray gauge. Also shown is the measured underflow density, plus the predicted underflow density based upon extrapolation of the bed density profile.

the position of the natural γ-ray gauge with respect to the moving rake. The gauge was inserted through the thickener lid just outside the feedwell (3.75 m from the centre) and met the conical floor 0.94 m above the level of the underflow take-off. The bottom of the gauge rested on the sloping floor during measurements, but had to be raised twice during each rake revolution to clear the torque arms and cables.

The measured bed density profile showed a smooth increase in solids concentration with increasing depth, which was rapid in the first metre of the bed and more gradual thereafter, reaching 0.130 volume fraction solids (VFS), i.e. 416 g l^{-1}, at a bed depth of 4 m. The underflow solids concentration (equivalent to a bed depth of 5 m) under these conditions was 0.19 VFS (610 g l^{-1}). This value was significantly greater than that predicted (0.133 VFS, 425 g l^{-1}) from a smooth extrapolation of the bed density profile curve as seen in Fig. 7. Thus there was a discontinuity (a jump) in the rate of increase of concentration with depth within the last (bottom) 1 m of the cone.

However, between rake revolutions, the natural γ-ray gauge did not detect any discontinuity down to the floor. The dewatering action of the rake (producing denser material), would have extended along the full length of the rake, but was restricted to a relatively narrow strip (perhaps a few metres wide) beneath and around the blades, i.e. the transport region [20]. The dewatered material in this strip would be transported continuously to the central outlet as fast as it formed, its width and mass being set by the relative rates of these two processes. It would have been missed when the natural gamma-ray gauge was raised to clear the rake (i.e. the gauge would have moved above it).

It is evident that there was a discontinuous and quite significant increase in solids concentration within the last 1 m of the bed. This can only be due to rake action and to the authors' knowledge this is the first reported observation of such concentration increase in a full-scale thickener.

3.2.2. Aggregate density measurements

The data in Fig. 7 and Table 2 demonstrate the importance of rake action on the full-scale, but do not indicate whether the enhanced sediment densification occurs by removal of inter or intra-aggregate liquor, or a combination of both. This was investigated using the FDA technique to determine how the density versus size relationship of the aggregates present in the underflow compared to that of aggregates formed in the feedwell. Samples were taken from the base of the feedwell and just prior to the underflow pump. These measurements were conducted on a different thickener to the one used to determine the bed density profiles shown in Table 2, but it had been previously shown through natural γ-ray gauge measurements to display a similar rake densification effect.

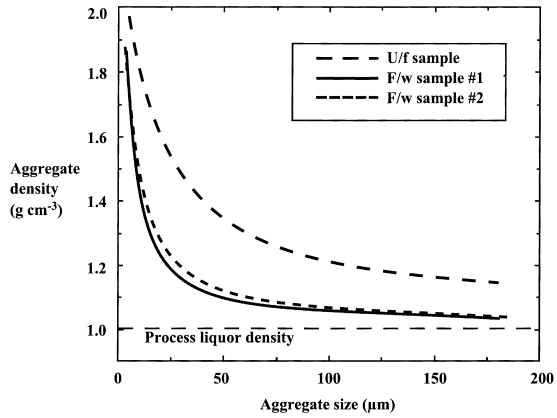

Fig. 8. Aggregate density versus aggregate size relationships obtained from FDA analysis of samples taken from the underflow and feedwell of a full-scale thickener.

The FDA results (Fig. 8) show distinct differences between the density versus size relationship of the individual aggregates present in the underflow sample compared to those of two feedwell samples (taken 24 h apart). For example, the average effective density of 100 μm aggregates present in the underflow is 1.22 g cm^{-3}, whereas that of both feedwell samples is 1.06 g cm^{-3}. This corresponds (using a particle density of 2.5 g cm^{-3}) to an average volume fraction solids of 0.147 and 0.04 for 100 μm aggregates within the underflow and feedwell samples, respectively. In other words, 100 μm underflow aggregates contain on average six parts water to one part solid (by volume) compared to 24 parts water to one part solid for 100 μm feedwell aggregates. While the assumptions made for this calculation may influence the absolute numbers, it is clear that the aggregates

Table 2
Comparison of measured underflow solids concentration to that predicted from the measured bed density profile obtained under a number of different operating conditions[a]

Profile	Bed height (m)	Underflow solids concentration					
		Projected		Measured		Difference	
		(VFS)	(g l^{-1})	(VFS)	(g l^{-1})	(VFS)	(g l^{-1})
No. 1	5.0	0.133	425	0.190	610	0.0494	185
No. 2	4.6	0.147	470	0.181	580	0.0342	110
No. 3	5.4	0.145	464	0.175	560	0.0301	96
No. 4	5.3	0.156	500	0.184	590	0.0283	90
No. 5	4.9	0.133	425	0.180	576	0.0465	151

[a]Data for profile no. 1 is shown in full in Fig. 7.

formed in the feedwell of this thickener densify significantly during their passage through the bed and into the underflow through removal of intra-aggregate liquor.

Unfortunately it was not possible to obtain samples of the sediment from just above the raking region in this full-scale thickener. FDA measurements on such samples would have allowed the extent of densification induced by compression from the weight of the overlying bed to be distinguished from the extent of densification induced from the action of the rake. It was observed in the laboratory column experiments with kaolin that a bed of 0.3 m causes very little aggregate densification (Fig. 6), implying sediment densification at this stage is only due to removal of inter-aggregate liquor. Whether this continues to be the case for beds of up to 4 m or more which are often used on the full-scale cannot be determined from the data reported here. However, what is clear is that aggregates reporting to the underflow have structures significantly denser than those formed in the feedwell.

4. Conclusions

Bed density profile measurements using a continuous laboratory-scale column have demonstrated that the hydrodynamic conditions prevailing during flocculation have an important affect on the consolidation behaviour of the sediment and the underflow density achieved under given operating conditions. This influence reflects that aggregates of different structure are formed with different hydrodynamic conditions during flocculation, and highlights the importance of optimising feedwell design on the full-scale.

Bed density profile measurements from the laboratory column and from a full-scale thickener have quantified the key role played by rake action in the densification of sediments. In all cases investigated, the densification achieved by the rake action dramatically exceeded that which could have been achieved through bed compression alone.

Measurements of the relationship between aggregate density and aggregate size for bed samples taken from both the laboratory column and a full-scale thickener have shown that rake action leads to significant aggregate densification through removal of intra-aggregate liquor. Removal of intra-aggregate liquor is the key to the formation of dense but pumpable sediments in industrial practice.

Acknowledgements

The support that has been provided by the following companies for the AMIRA ‘Improving Thickener Technology’ projects is greatly appreciated: Alcoa of Australia, Baker Process, Bateman Process, BHP, Billiton, Centaur Mining & Exploration, Cytec, Dorr-Oliver, Hydro Aluminium, Kidd Creek Mines, MERIWA, MIM Holdings, Nabalco, Nalco Chemicals, North Limited, Pasminco, Queensland Alumina, Queensland Nickel, Rio Tinto, SNF, Supaflo Technologies, Western Mining, Westralian Sands, Worsley Alumina. This research has also received support from the Australian Government’s Cooperative Research Centre (CRC) program, through the AJ Parker CRC for Hydrometallurgy. This support is gratefully acknowledged. Ben Fletcher and Warren Jones from CSIRO made important contributions to the experimental aspects of this work.

References

[1] K.P. Galvin, A.G. Waters, Powder Techn. 53 (1987) 113.
[2] E.W. Comings, Ind. Eng. Chem. 32 (1940) 663.
[3] M. Muniz, H. Berthiaux, A. Gutierrez, et al. Powder Techn. 96 (1998) 267.
[4] L.G. Eklund, A. Jernqvist, Chem. Eng. Sci. 30 (1975) 597.
[5] M.V. Maljian, J.A. Howell, Trans. IChemE 56 (1978) 56.
[6] D.C. Dixon, Chem. Eng. Sci. 43 (1988) 392.
[7] P. Kos, J. Am. Water Works Assoc. 69 (1977) 272.
[8] W.R. Richmond, R.L. Jones, P.D. Fawell, Chem. Eng. J. 71 (1998) 67.
[9] P.D. Fawell, W.R. Richmond, R.L. Jones, et al., Chem. Aust. 64 (2) (1997) 4.
[10] J.B. Farrow, J.D. Swift, Proceedings of the Fourth International Alumina Quality Workshop, vol. 2 Darwin, Australia, 2–7 June, 1996, p. 355.
[11] J.B. Farrow, J.D. Swift, Int. J. Min. Process. 46 (1996) 263.
[12] J.B. Farrow, L.J. Warren, in: B. Dobias (Ed.), Coagulation and Flocculation—Theory and Application, Marcel Dekker, New York, 1993, p. 391 Chapter 9.
[13] J. Happel, H. Brenner, Low Reynolds Number Hydrodynamics, Noordhoff International, Leyden, 1973, p. 223.
[14] R. Hogg, R.C. Klimpel, D.T. Ray, Miner. Metall. Process. 4 (2) (1987) 108.
[15] L.A. Glasgow, J.P. Hsu, Part. Sci. Technol. 2 (3) (1984) 285.
[16] L.A. Glasgow, Chem. Eng. Prog. 85 (8) (1989) 51.
[17] P.J. Mathew, in: S.M. Rao, et al. (Eds.), Industrial Applications of Radioisotopes and Radiation, Wiley Eastern, New Delhi, 1986, p. 154.
[18] P.J. Mathew, Australian Patent No. 555721, Feb. 1983.
[19] P.J. Mathew, Australian Patent No. 81166, Nov. 1987.
[20] O.E. Albertson, R.W. Okey, Water Env. Technol., Jan. (1992) 52.